Presented at the 28th European PV Solar Energy Conference and Exhibition, 30 Sept. – 04 Oct. 2013, Paris, France

INFLUENCE OF ARGON FLOW RATE ON MELT CONVECTION AND INCORPORATION OF SIC IN MULTICRYSTALLINE SILICON

C. Schmid, M. Schumann, F. Haas, S. Riepe
Fraunhofer Institute for Solar Energy Systems (ISE)
Heidenhofstr. 2, D-79110 Freiburg, Germany
Phone +49 (0)761–4588–5640, Fax +49 (0)761–4588–9579;
e-mail: claudia.schmid@ise.fraunhofer.de

ABSTRACT:
The influence of the argon flow rate on the melt convection pattern and precipitate formation has been investigated by global, axisymmetric time-dependent simulations for varied argon flow rates and test crystallisations of G1 sized ingots. The simulations include calculation for the global heat transfer, the gas/melt convection, the melt-crystal interface determination, impurity transport and precipitation. The simulation results have been compared with precipitate distribution and impurity profiles in the test ingots. The ingots were prepared in a laboratory VGF furnace with a modified support crucible system. It can be shown that the argon flow rate has a significant impact on the melt convection pattern and thus the impurity distribution in the solidified ingots. This determines the formation and amount of SiC precipitations especially in the upper part of the ingots.

Keywords: Crystallisation, Simulation, Multicrystalline Silicon, Argon Flow Rate

1 INTRODUCTION

About 50 % of all solar cells are based on multi-crystalline silicon (mc-Si) crystallised by directional solidification. The electrical and mechanical properties of mc-Si and therefore the solar cell performance are dependent on the distribution of impurities. Carbon and nitrogen are very important impurities with respect to the crystallisation process and can have high concentration levels in the Si melt up to the solubility limits. Sources for carbon are predominantly the graphite parts in the furnace such as graphite support crucible, heater and insulation. Carbon can be incorporated into the Si melt in form of carbon monoxide (CO) via the furnace atmosphere during the crystallisation process. The main source for nitrogen in the Si melt is the crucible coating.

If the carbon or nitrogen concentration in a melt volume exceeds the solubility limit silicon carbide (SiC) and silicon nitride (Si_3N_4) precipitates can be formed, respectively [1]. These precipitates can cause damages and wire ruptures during the wire sawing process [2] or shunts in the processed solar cell [3].

To reduce the incorporation of additional carbon from the gas atmosphere into the silicon the melt surface is flushed with argon. This argon flow has several effects. Li et al. [4] showed that the argon flow rate has an impact on convection pattern and temperature distribution especially in the upper part of the silicon melt. Bellmann et al. [5] investigated the effects of melt convection pattern and melt-crystal interface shapes on the segregation of impurities. They showed that the shape of the interface influences the velocity distribution of the melt in front of the interface and therefore affects the impurity distribution in the solidified silicon.

In the presented paper the influence of the argon flow rate on the melt convection and the formation of SiC precipitates are investigated on the basis of numerical simulation and experiments in a Vertical Gradient Freeze (VGF) furnace.

2 EXPERIMENTAL AND SIMULATION DETAILS

2.1 Experiments

Three test ingots of the size G1 with 14 kg silicon feedstock and the dimensions 220 x 220 x 130 mm^3 were crystallised in a laboratory VGF furnace by directional solidification. The Si was melted and solidified in an industrial type quartz crucible, coated with silicon nitride lining. The support crucible system consisted of surrounding graphite plates and a graphite top cover and had been modified compared to industrial like systems in such a way that the thermal conductivities are different over the height (Fig. 1). The crucible system was flushed with argon for the whole process; the argon flow rate for the solidification process itself was varied for the three ingots with 2 slm, 6 slm and 10 slm. All other parameters (e.g. the thermal process) remained the same.

After crystallisation the edge parts of two opposing sides were cut and the cross section surfaces mechanically polished for further investigation. The ingots were inspected for inclusion and precipitate distribution by Infrared transmission. A 2 mm thick slice adjacent the investigated cross section was prepared for measurements of substitutional Carbon (C_s) and interstitial Oxygen (O_i) via the Fourier transformed Infrared measurement technique (FTIR).

2.2 Simulation

Time-dependent 2D simulations of the solidification processes in the furnace were made with the software BasicCGSim (STR GmbH). The axisymmetric simulations describe the crystallisation processes for varied argon flow rates (2 slm, 6 slm and 10 slm) and include the calculation of heat transfer, gas/melt convection, melt-crystal interface shape determination, species transport and formation of SiC and Si_3N_4 precipitates.

The mathematical model of heat transfer, convection and chemistry are implemented in the software and described in [6].

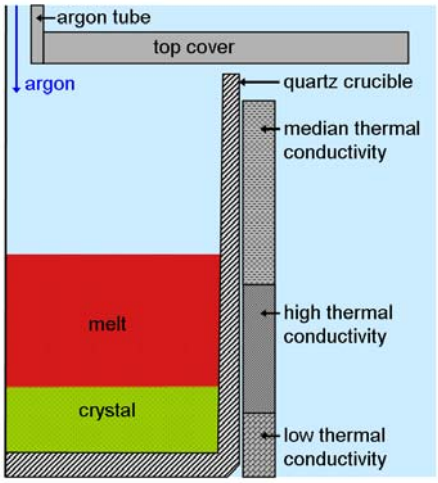

Figure 1: Schematic half cross section of the crucible system including quartz crucible with silicon and modified support crucible for the simulated processes.

3 RESULTS

3.1 Melt convection patterns

The simulations show a concave interface shape at the beginning of the crystallisation. For 2 slm and 6 slm argon flow rate two melt convection vortices occur (Fig. 2). The upper one transports silicon melt from the surface downwards into the melt volume at the crucible centre and upwards at the crucible wall. In contrast, the Si melt within in the region of the lower vortex goes up in the centre and down at the crucible wall. For 10 slm argon a small third vortex appears near the melt surface in the crucible centre. The melt flow direction here is determined by the argon stream driving the Si melt along the surface for a short distance before hitting the upper large vortex. No significant differences of the velocity distribution due to the different argon flow rates can be observed at this stage (Fig. 2).

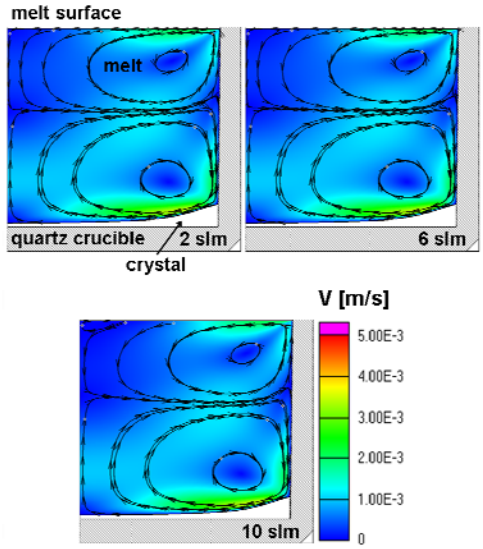

Figure 2: Simulated velocity distribution and convection pattern in silicon melt for 2 slm (top left), 6 slm (top right) and 10 slm (bottom) argon flow rate at early crystallisation stage.

With advancing crystallisation the melt convection patterns show greater differences (Fig. 3). With approx. 50 mm solidified there are still two vortices with 2 slm argon. With 6 slm argon a small third vortex develops at a centre position near the melt surface. With 10 slm argon this small third vortex and the lower vortex merge to a big one.

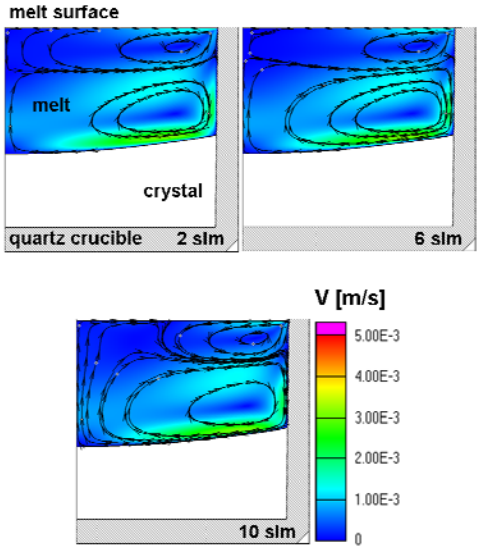

Figure 3: Simulated velocity distribution and convection pattern in silicon melt for 2 slm (top left), 6 slm (top right) and 10 slm (bottom) argon flow rate with approx. 50 mm solidified.

This process "development of third vortex and fusion with lower vortex" occurs for 2 slm and 6 slm at different and later crystallisation times: For 2 slm this happens when approx. 85 mm of the ingot has been solidified, for 6 slm at approx. 60 mm ingot solidified.

At approx. three quarter solidified fraction the previously lower vortex has almost completely replaced the previously upper vortex. Only a very small residual vortex can be observed near the crucible wall for all three argon flow rates (Fig. 4). From this solidification height on the velocity distribution is clearly influenced by the argon flow rate. For 10 slm the velocity distribution is significantly higher at the melt surface than for 2 slm and 6 slm.

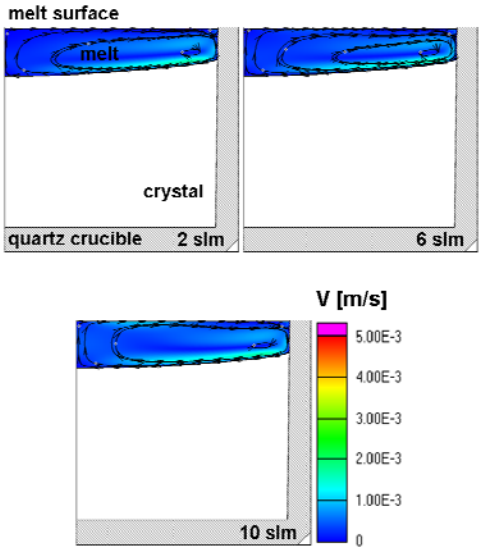

Figure 4: Simulated velocity distribution and convection pattern in silicon melt for 2 slm (top left), 6 slm (top right) and 10 slm (bottom) argon flow rate with approx. 100 mm solidified.

3.2 Impurity distribution

The three test ingots show SiC and Si_3N_4 precipitates starting from median height of the ingot (Fig. 5). The quantity of precipitates decreases with increasing argon flow rates. With 2 slm argon the whole upper half of the ingot depict precipitates, with 6 slm argon there are less precipitate rich areas and with 10 slm argon only an approx. 1.5 cm wide belt of precipitates can be observed. The close up shown in the lower right part of Fig. 5 indicates that both needle-like Si_3N_4 and more blocky SiC precipitates occur.

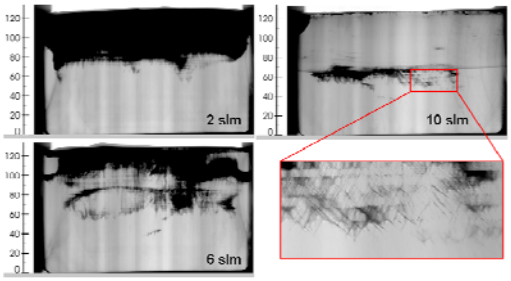

Figure 5: IR images of the three test ingots. Top left 2 slm, bottom left 6 slm, top right 10 slm and bottom right close up of some precipitates (the absolute ingot height in mm is shown on the left side of each image)

The FTIR measurements of substitutional carbon (C_s) show much higher values for 2 slm argon flow rate (Fig. 6). The graph doesn't follow an exponential increase as expected by the Scheil's progression. The values from the ingot with 6 slm are only slightly higher as those for the ingot with 10 slm.

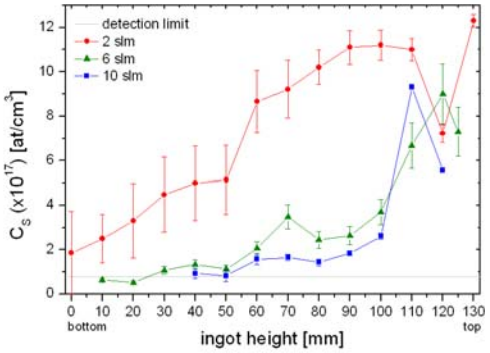

Figure 6: FTIR measurement of substitutional carbon (C_s)

The oxygen distribution over ingot height, measured near the ingot centre, decreases with increasing argon flow rate (Fig. 7). This indicates an increasing SiO transport away from the melt surface as expected for the argon flushing.

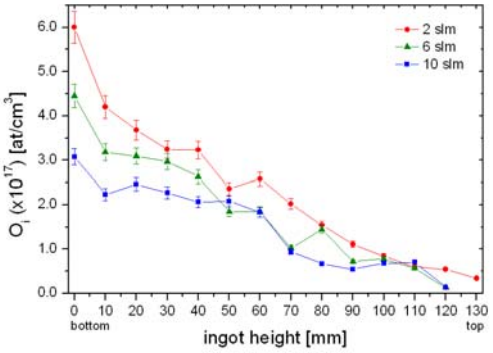

Figure 7: FTIR measurement of interstitial oxygen (O_i)

The simulated CO distribution directly above the melt surface, averaged over the melt area, decreases with increasing argon flow rate (Fig. 8). With 2 slm argon flushing the values are significantly higher than with 10 slm argon. For 6 slm, the CO concentration is only slightly higher

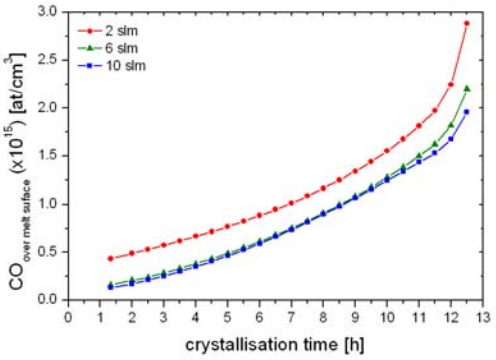

Figure 7: Simulated averaged carbon monoxide (CO) distribution at the melt surface for 2, 6 and 10 slm.

4 DISCUSSION

The simulations show that the flow rates of argon have an impact on the melt convection patterns and velocity distributions in the upper part of the melt volume (see Fig. 1 to 3). With higher flow rates more vortices develop at earlier solidification points. The influence of the argon flow rate increases with advancing solidification. The variations in convection pattern lead to a different mixing behaviour of the melt and hence to a different distribution pattern of impurities.

The CO distributions over the melt surface (Fig. 7) imply that with higher argon flow rates the flushing of the melt surface is more effective due to higher velocities and amounts of argon. Therefore fewer carbon monoxide is incorporated into the melt over the melt surface with higher argon flow rates. The little differences in the CO distribution as well as in the FTIR measurements (Fig. 6) between 6 slm and 10 slm indicate that there is an optimum flow rate between these values in terms of flushing and transport of CO to the melt surface from the graphite parts in the furnace.

The IR images (Fig. 5) show different amounts of precipitates. Analysis of the close up image imply that the precipitates in these regions are dominated by Si_3N_4 in the lower part and by SiC in the upper part of the precipitate rich areas in the ingot. The formation of the precipitates starts at different solidification points for different argon flow rates. With 10 slm the main formation starts when approx. 50 mm are solidified. This correlates with the changes in the melt convection pattern which take place later in the process for 6 slm and 2 slm argon flow rate.

5 CONCLUSIONS

The numerical simulations show that the flushing effect on the melt surface increases with higher argon flow rates. It can be concluded that higher argon flow rates can help to reduce the incorporation of carbon via CO from the furnace atmosphere into the melt.

The argon flow rate also influences the melt convection pattern and the velocity distribution in the upper melt volume part. The changes in melt pattern are also dependent of the furnace geometry respectively the support crucible setup.

It can be concluded that higher argon flow rates can reduce or avoid the formation of SiC precipitates.

6 ACKNOWLEDGEMENT

The author wants to thank Jan Holtkamp (Fraunhofer ISE) for preparing the FTIR measurements and STR for helpful discussions.

This work was funded by the German Federal Ministry for the Environment, Nature Conservation and Nuclear Safety (Contract Number 0325491) and by the Fraunhofer Society within the project Silicon Beacon.

7 REFERENCES

[1] L. Liu, S. Nakano, K. Kakimoto, J. of Crystal Growth 310 (2008) 2192–2197

[2] G. Du, L. Zhou, P. Rossetto, Y. Wan, Solar Energy Materials & Solar Cells 91 (2007) 1743-1748

[3] O. Breitenstein, J.P. Rakotoniaina, M.H. Al Rifai, M. Werner, Prog. Photovolt: Res. Appl. 12 (2004) 529-538

[4] Z. Li, L. Liu, W. Ma, K. Kakimoto, J. of Crystal Growth 318 (2011) 298 - 303

[5] M.P. Bellmann, M. M'Hamdi, J. of Crystal Growth 362 (2013) 93 - 98

[6] CGSim, User Reference Guide 12.2, 2003-2012, STR IP Holding, LLC, Richmond, VA, USA